Exciton Coupling in the Photosystem I Reaction Center

Godfrey S. Beddard†

School of Chemistry, University of Leeds, Leeds LS2 9JT, U.K.

Received: April 16, 1998; In Final Form: August 18, 1998

The electronic properties of the photosynthetic reaction center of photosystem I have been investigated on the basis of the X-ray structure of *Synechococcus elongatus*. The exciton coupling between nearest neighbors is calculated to be of a similar magnitude and about 330 cm^{-1}. To match the calculated to the experimental transient difference spectra ($P_{700}^+ - P_{700}$) and ($A_0^- - A_0$) an angle of 40 ± 10° between the Q_y transitions of the special pair chlorophylls was required. The effect of separating and translating the special pair chlorophylls was also investigated. The localizing effect on the exciton states of adding disorder to the intermolecular couplings was studied.

1. Introduction

The recent 4 Å resolution X-ray determination[1,2] of the structure of the photosystem I (PSI) reaction center (RC) of the photosynthetic cyanobacterium *Synechococcus elongatus* allows a preliminary calculation of its electronic properties. As with the reaction centers of photosynthetic bacteria, PSI contains six pigments and two secondary electron acceptors arranged in a well-defined but approximate C_2 symmetric structure in the protein. Conventionally the two closest chlorophylls (Chl) are called the "special pair", the next two, one on either side of the special pair, are called the accessory pigments, and the next two are the primary electron acceptors. In PSI the absorption of the reaction center occurs at ∼700 nm, and the pigments involved are called P_{700}. Conventionally this absorption would be associated with the special pair although experiments so far do not indicate exactly from which pigments the absorption arises.

There have been several calculations of the electronic structure of the bacterial RC[3−13] whose structure was determined a few years ago,[14,15] but there has only been a preliminary report of the electronic structure of PSI.[16] The electronic structure of the reaction center of photosystem II has also been less studied than those of bacteria, most notably by Durrant et al.[17] using a structure modified from that of bacteria by increasing the special pair separation by 2.8 Å. They suggest a similar size of exciton coupling between each pigment and its near neighbor and exciton states partially delocalized over the pigments.

The structure of the PSI reaction center is shown in Figure 1a; P1 and P2 are the special pair, C3, C4 the accessory Chls, and A5 and A6 the primary electron acceptors A_0. The secondary acceptors are not shown in Figure 1 but are situated between A5/A6 and the iron sulfur center, which is ∼30 Å above P_{700} and 20 Å from A5 and A6. While there is clearly a great similarity to that of the bacterial RC (Figure 1B), there are also important differences. One is that the pigments are all Chl-a, not bacteriochlorophyll (BChl) or bacteriopheophytin (BPh), and the other is that the accessory Chls (C3, C4) are oriented differently compared to their bacterial equivalents (Figure 1). Note that Figure 1B shows the geometry of a hypothetical bacterial RC in which BChl and BPh are replaced by Chl but which otherwise has the bacterial RC geometry.

† E-mail: Godfrey.Beddard@chem.leeds.ac.uk.

The absorption spectrum of the PSI RC was calculated in three oxidation states by generating the MO's of the Chl, Chl^+, and Chl^- molecules, performing configuration interaction in the "four orbital" model in which the major transitions involve the top two filled orbitals and the lowest two unfilled orbitals.[18] The pairwise exciton coupling between each pair of molecules was then calculated using the SCF−CI method described by Warshel and Parson.[19] In each pair of interactions the off-diagonal terms in the configuration matrix describe the mixing of the local and charge-transfer transitions. These matrices were combined and diagonalized to obtain the eigenvalues and hence spectrum of the complete RC. The spectrum of the six-molecule structure was modeled and also the difference spectrum $P_{700}^+ - P_{700}$ with one of the special pair as Chl^+ and also the spectrum of $A_0^- - A_0$ with the acceptor as Chl^-.[16,20] The relative orientation of the Chl's *y* axis, which lies in the plane containing the pyrrole nitrogen atoms, is unknown from the X-ray data so that free rotation of the molecules in that plane was allowed. Consequently in the calculation many rotation angles about the *z* axis were examined so as to find those best representing the transient absorption data.

2. Method

2.1. Calculation of Transition Energies. The visible transitions of Chl are conventionally labeled Q_x, Q_y, B_x, and B_y. The lowest $\pi\pi^*$ transition (Q_y) is, in ether, at 662 nm, and a weaker Q_x band occurs at 578 nm. The $B_{x,y}$ transitions are found in a broad band at ∼430 nm.[21] Using coordinates taken from the X-ray structure of ethyl chlorophyllide·H_2O,[22] the eigenvalues were calculated from an ab initio calculation using Gaussian-94[23] in an all-electron Hartree−Fock calculation using a 3-21G basis set. The calculated transition energies (ΔE) produced were larger than those observed experimentally, a discrepancy that has been noted before, both for porphyrins and chlorins,[19,24] but which could be matched to the Chl absorption spectrum with the formula $\Delta E' = 0.684\Delta E - 1550$ (cm^{-1}). The energies $\Delta E'$ were used only for comparison of the calculated spectra with experiment. The transition dipole magnitudes and directions compared moderately well with experiment,[16,25−27] of which those of the Q_y transition are the most important. The Q_y transition was observed [27] to lie at

10.1021/jp981895t CCC: $15.00
Published on Web 12/03/1998

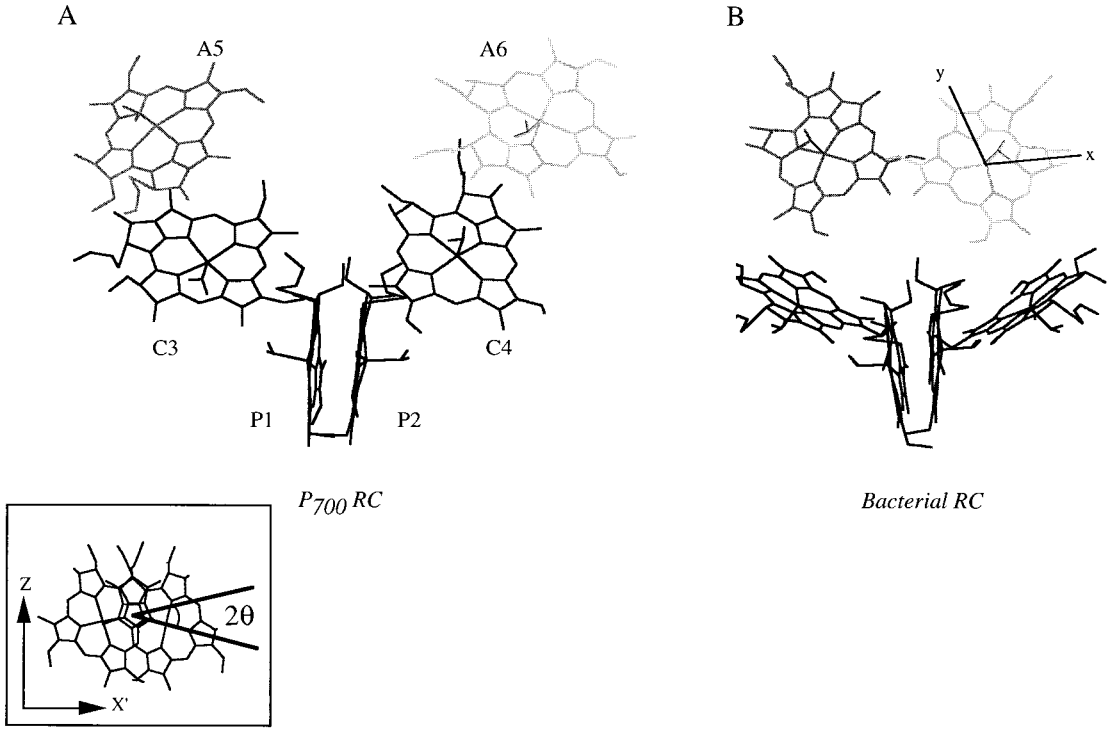

Figure 1. (Left) Structure of the PSI reaction center based on the X-ray data of Krauss et al.[46] (Right) Hypothetical structure of a bacterial RC[30] with Chl instead of BChl or BPh. (Inset) Side view of the special pair P1, P2 in PSI; the horizontal axis, x', is the displacement as used in Figure 4.

77.5° to the x axis and was calculated at 84.1°.[16] The observed[26] and calculated[16] dipole strengths are 26 and 32 D^2, respectively.

2.2. Exciton Coupling. Using the method of Warshel and Parson,[19] the exciton interaction was calculated between the four local states Ψ_i on molecule "A" with states Ψ_k on molecule "B" leading to eight new states. The molecular wave functions, ϕ_1 or ϕ_2, were constructed as a linear combination of orbitals

$$\phi_{1i} = \sum_s a_{i,s}\chi_s \quad \text{and} \quad \phi_{2i} = \sum_t a_{i,t}\chi_t \tag{1}$$

where labels s and t on the expansion coefficients $a_{i,s}$, $a_{i,t}$ refer to different molecules and χ is an orbital on atom s or t. The interaction matrix between each pair of molecules is written in block form as[19]

$$U = \left(\begin{array}{cc|cc} \Delta E^a & U^{ex} & \multicolumn{2}{c}{U^{loc,ct}} \\ U^{ex} & \Delta E^b & & \\ \hline \multicolumn{2}{c|}{U^{ct,loc}} & U^{ct} & 0 \\ & & 0 & U^{ct} \end{array}\right) \tag{2}$$

where U^{ex} is the 4 × 4 matrix of exciton interactions between molecules a and b and $\Delta E^{a,b}$ are diagonal matrices of local transition energies. The pair of molecules also has four principle charge-transfer (CT) interactions U^{ct} in which an electron is transferred from an orbital of one molecule to that of another. These transitions[19] can also interact with the local transitions (Q_y, etc.) of the molecule, $U^{ct,loc}$. The electrochromic interaction takes the form[3]

$$\Delta(\text{elec})_i^b = -\sum_n c_{i,a}^2 \sum_{s,t} a_{q,s}^2 (a_{a1,s}^2 - a_{a2,s}^2)\gamma_{s,t}/D \tag{3}$$

where $\Delta(\text{elec})_i^b$ is the energy correction for the transition i on molecule b. The dielectric constant D was given a value of 3. The subscript label q refers to orbital q of atom s and depends on whether the transition involves P^+ or A^-. The parameter γ estimates the electron−electron repulsion integral; see Parson and Warshel[3] for further details.

2.3. Spectral Simulations. The spectra were simulated by using the eigenvalues and eigenvectors obtained from a diagonalization of a matrix of all molecular pair interactions and using the spectrum of Chl-a as a basis.[28] However, the match between experiment and theory can never be exact at wavelengths less than the S_0-S_1 (0−0) transition as no vibronic terms were included in the exciton calculation but are observed in the Chl spectrum. These features will therefore only be accounted for approximately in the simulation. The spectra were also satisfactorily simulated by adding random perturbation energies to the elements of the exciton interaction matrix (eq 2) and then using the numerical averaging method of Fidder at al.[29] The Hamiltonian has the form

$$H = \sum_i |i\rangle(\hbar\omega_0 + \sigma_i)\langle i| + \sum_{i\neq k} |i\rangle(V_{ik} + \delta V_{ik})\langle k| \tag{4}$$

where the ideal transition energies are represented by $\hbar\omega_0$, σ_i, and δV_{ik}, respectively, represent the diagonal and off-diagonal disorder energies, and V_{ik} is the coupling between molecules. This has the form $V_{ik} = V/|r_i - r_k|^3$, where r are the positions of the molecules. The disorder energies σ were sampled from a Gaussian distribution of fwhm = 2 ln (2)σ, and to sample the distribution properly 5000 matrices were diagonalized and the results then averaged at each magnitude of the disorder. Only static disorder was included in eq 2 and only the U^{ex} quadrant was used, but the calculation involved all four transitions on each of six pigments.

3. Results and Discussion

3.1. Comparison with Experimental Difference Spectra. The nitrogen atoms in the Chls were superimposed to minimum error upon the coordinates of the nitrogen atoms obtained from

TABLE 1: Exciton Coupling Energies (to Nearest cm^{-1})[a]

	P2	C3	C4	A5	A6
P1	**334** (**12**)	**−296**	51	45	3 {80}
P2	0	86 (−222)	**−303** (−248)	−3 (69)	−33 (68) {21}
C3		0	73	**368**	−20 {9}
C4			0	−28	**367** {−44}
A5				0	18 {−58}

[a] The values in brackets are those energies when the RC contains either (P_{700}^+) or {A_0^-}. Near-neighbor couplings are in bold type. In the notation of Krauss: P1 ≡ eC1′, P2 ≡ eC1, C3 ≡ eC2, C4 ≡ eC2′, A5 ≡ eC3, A6 ≡ eC3′.

the PSI X-ray data. The spectrum of PSI was then calculated using eq 2 with all six molecules included, and as a test a seventh and eight Chl were added as they lie some way between the main antenna and the RC.[1] These Chls are not shown in Figure 1 for clarity, since they would partly obscure A_0 (A5, Figure 1) and A_0' (A6, Figure 1) to which they have a coupling of ∼60 cm^{-1}. These pigments changed the difference spectrum only slightly and were not included in further calculations.

The effect of charge-transfer interactions (U^{ct}, eq 2) on the calculation was also found to be very small (<5 cm^{-1}) for all pairs of molecules except for the special pair where it is ∼150 cm^{-1}, using a "typical" protein dielectric constant of 3, and produced only a 2 nm shift in wavelength of the lowest transition.

The PSI spectrum was calculated at several different orientations of the Chl molecules by rotating them in the plane of the N atoms, i.e., about their *z* axes. The angle θ between the special pair Q_y transitions in bacterial RC's is ∼38°,[30] and a similar angle has been suggested from experiments on PSI.[31] Simulating the PSI difference spectrum ($P_{700}^+ - P_{700}$) is difficult as only this spectrum is known experimentally and not the P_{700} and P_{700}^+ ground states. Therefore starting at 40° between the special pair (see insert Figure 1), which is close to the experimentally estimated angle,[31] the rotation angles about a molecule's *z* axis were systematically varied for each of the accessory and A_0 Chls, and P_{700}, P_{700}^+ and A_0^- were calculated at each angle. The calculation was simplified by keeping the structure approximately symmetrical. The best geometry was determined by comparing the difference spectra ($P_{700}^+ - P_{700}$) and ($A_0^- - A_0$) with those obtained experimentally,[20 32] and the optimum estimated coupling values for the RC are shown in Table 1.

The experimental and calculated difference spectra of P_{700}^+ and A_0^- are shown in Figure 2A,B, curves 1 and 2, respectively; a more detailed comparison is given elsewhere[16] and is only outlined here. In general the calculated $P_{700}^+ - P_{700}$ spectrum has the same form as the picosecond experimental data, the bleaching transient at ∼696 nm is reproduced well, but the smaller features at ∼655 and 670 nm are at shorter wavelengths than observed experimentally. The calculated and experimental $A_0^- - A_0$ spectrum (Figure 2B) are also in good agreement. This calculated spectrum is sensitive to electrochromic effects, whereas these interactions have only a small effect on P_{700}^+, and if they are not included in $A_0^- - A_0$ a large bleaching occurs both at 680 and ∼695 nm. A similar two peaked difference spectrum can also be reproduced by rotating the angles between P_1 and P_2 away from ∼40° even when the electrochromic terms are included. Hastings et al.[33] have suggested that there may be another transient in the $A_0^- - A_0$ spectrum, due to the second A_0 pigment if it is assumed that electron transfer is not unidirectional. This effect is expected to be seen in our model for although the coupling in P_{700} involves all molecules to varying degrees, the different disposition of A5 and A6 does lead to slightly different A_0^- spectra depending on which of these molecules the electron is placed, but our simulations are not accurate enough given the experimental uncertainty in geometry to confirm such a subtle effect.

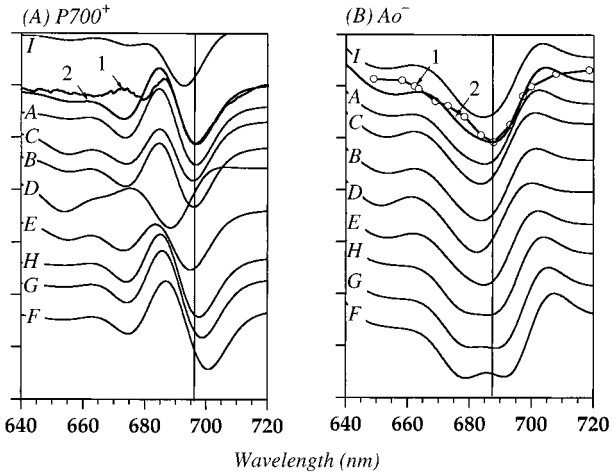

Figure 2. Calculated and experimental difference spectra (A) $P_{700}^+ - P_{700}$ and (B) $A_0^- - A_0$. The experimental data (line 1A) is taken from ref 20 and line 1B from ref 32. The best fit calculated lines are A2 and B2. Lines A−H refer to spectra discussed in the text calculated at coordinates A−H as shown in Figure 4. Lines *I* are calculated as for lines 2 but with 55° instead of 40° between Q_y dipoles; see text for details. The vertical line is at the minimum experimental bleach and is intended as a guide to the eye.

The noticeable feature of the coupling between the pigments, Table 1, is the similarity of the magnitude of the values between closest pairs; electronically the identity of a "special pair" is not particularly obvious, unlike the bacterial RC where the coupling between the special pair is ∼750 cm^{-1} in *Rhodopseudomonas viridis* and 1050 cm^{-1} in *Rhodobacter sphaeroides* at 4.2 K,[34] and which is also much stronger than that between the other pigments. This size of the pairwise coupling in PSI is not entirely unsurprising as the plane-to-plane separation in bacterial RC's is ∼3.5 Å, but 5 Å in PSI and possibly larger in PSII.[35] Table 1 also shows the coupling energies in the RC containing P_{700}^+ and A_0^-. The main difference occurs between the charged species, P_{700}^+ or A_0^-, and the adjacent pigment. In P_{700}^+ this coupling is reduced to only 12 cm^{-1}, and its spectrum shows the effect of this as a narrowing relative to the "neutral" RC.[16] A transition is also present at ∼820 nm in both types of difference spectra but is so weak and shifted in energy that it does not affect the transitions in the 650−700 nm region. This absorption was attributed[16] to a similar transition occurring in the Chl^+ (and Chl^-) absorption spectrum.[36]

Figure 3A shows the normalized amplitudes a_{is}^2 of the exciton states in P_{700}. The amplitudes are given by an equation similar to eq 1 when χ represent the exciton states. The lowest energy state is labeled 1 and shows that here the special pair and accessory pigments share about equal amplitudes but acceptors A_0 and A_0' have comparatively low amplitudes. The next higher energy state has little amplitude on P1 and P2 and similar amplitudes on the other pigments. Overall the pattern of amplitudes is *very* approximately that of a linear hexatriene. Figure 3B shows the energy splittings of states 1 to 6 relative to Chl in the protein and which is in turn displaced by Δ cm^{-1} from solution (15 105 cm^{-1} or 662 nm), which taken to be zero.

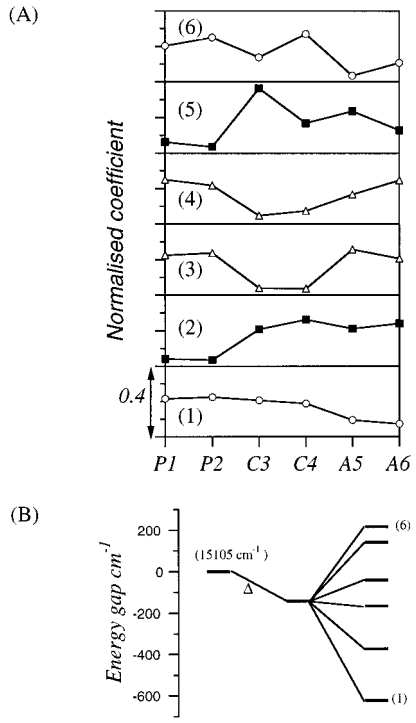

Figure 3. (A) Normalized amplitudes of the exciton states a_{is}^2 vs site. See Figure 1 for labels. (B) Energy (cm^{-1}) of the exciton states relative to Chl in protein, which is displaced by △ from solution at 15 105 cm^{-1} or 662 nm.

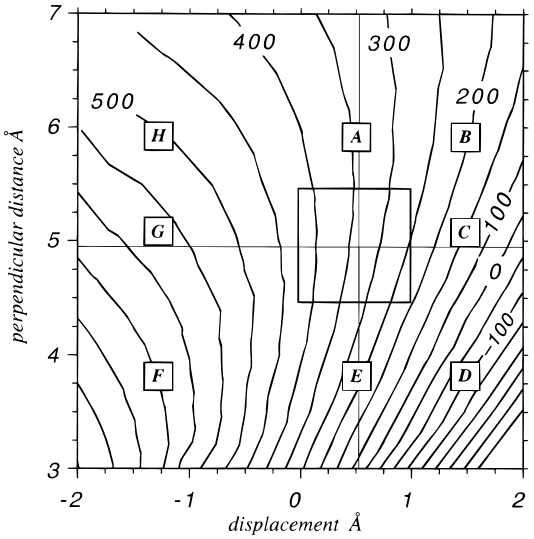

Figure 4. Contour plot of the special pair (P1−P2) coupling energy (cm^{-1}) vs displacement and separation. Displacement along the *x*′ direction (inset Figure 1A) maintains the same interplanar separation; separation increases interplanar distance. The thin lines cross at the X-ray geometry; the square represents $\pm^1/_2$ Å uncertainty in the X-ray coordinates. Spectra calculated at points A−H are discussed in the text.

3.2. Modified Geometry. *3.2.1. Displacement and Translation of the Special Pair.* The X-ray structure is as yet known only to 4 ± 0.5 Å so that there is still some uncertainty in the interplanar separation and displacement. To test the importance of these parameters on the spectra produced, the coupling strength between P1 and P2 was calculated vs the perpendicular distance between rings and their *x* displacement, as shown in Figure 4. The calculated difference spectra at points labeled A−H are shown in Figure 2. In Figure 4 the square has a 1 Å side and represents estimated uncertainty in positions of the special pair. The measured X-ray geometry is at the intersection of the straight lines and center of the square. The perpendicular distance was measured between the mean of the N atoms position of one Chl to the best plane containing the nitrogen atoms on the other. The distance was not measured from the Mg atom as this does not sit in the plane of the Chl but about 0.3 Å toward the ligated water molecule. From the contour plot it is clear that the coupling changes less on separating the molecules compared to when they are translated past one another. This is understandable from the shape of the MO's as their overlap changes relatively more on translation than separation.

Calculation of spectra at positions A to H tests how much the geometry could be changed and still match the experimental data; the results are shown in Figure 2. The criteria used to match the spectra were that the bleaching wavelength be matched to experiment to within ±1 nm, as this is the experimental uncertainty, and that normalized spectral shape calculated vs experimental should be the same. The vertical lines (Figure 2) show the wavelength of the maximum bleach at 696 and 687 nm for P_{700}^+ and A_0^-, respectively. Lines 2 (Figure 2) are the best fits to both the experimental $P_{700}^+ - P_{700}$ and $A_0^- - A_0$ difference spectra, lines 1. Other pairs of spectra such as A, B, C, E (see Figure 4 for positions) have moderate fits but D, F, G, H poor fits. Spectra A, B, C, E each fit the main P_{700}^+ bleach, but the A_0^- bleach progressively moves to shorter wavelengths, by about 4 nm in curve B, which is significantly different to the experimental data. Spectra from position D and also F, G, H can be discounted as either one or both P_{700}^+ or A_0^- difference spectra fit poorly to the experimental data. These spectra were all calculated at 40° between Q_y axes. Lines I in Figure 2 show the effect of increasing this angle by 15° at the normal X-ray geometry. Both the P_{700}^+ and A_0^- difference spectra show a poorer fit to the data, and at larger angles the fit worsens.

The main conclusions to be drawn from these spectra are that to within the ±0.5 Å resolution of the X-ray data the calculated spectra will appear identical and that these data are consistent with the experimentally estimated angle between special pair Q_y dipoles of 40 ± 10°. At slightly larger or smaller special pair separations than the X-ray geometry (points A, E) the spectra are similar to one another and to that at the optimum position. At smaller or larger displacements (points D, F, G, H) the calculated spectra do not fit the experimental data at all well. When translated into coupling energy between the special pair the difference spectra are matched with a value of 330 (+200, −100) cm^{-1}.

3.2.2. Variation of the Angle between the Special Pair Q_y Transitions. As the angle between the Q_y dipoles of the special pair is varied the calculated dipole strength of the lowest energy transition changes as does the coupling energy. This is illustrated in Figure 5. At the estimated best geometry, as shown by the line at 40°, the coupling is almost at a minimum and the dipole strength almost at a maximum. In PSI there are antenna states absorbing at 712−720 nm, wavelengths that are 300−500 cm^{-1} below the P_{700} trap and from which uphill transfer to the trap must occur relatively slowly compared to exothermic transfer. Rotation of the special pair Chl by ±200° would make the trap the lowest energy state in the antenna RC complex. As the absorption cross section at this angle is almost zero such a trap would be disadvantaged relative to P_{700}, not only because of the small absorption cross section but also because the next highest transition occurs at a higher energy than would the lowest transition at the 40° geometry, i.e., at shorter wavelengths than 696 nm.

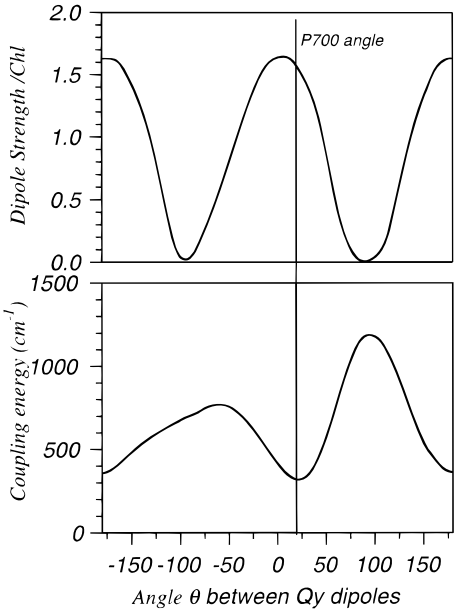

Figure 5. Coupling energy (cm^{-1}) and dipole strength (top) of P1 and P2 vs angle θ between Q_y dipoles measured in degrees. The vertical line represents the angle that best fits to experiment.

3.3. Effect of Coupling Size. If we make the reasonable assumption that the ideal RC should maximally accept energy from the antenna and store as much of this as possible as potential energy for the subsequent electron-transfer reactions, then surprisingly, it is not clear what the optimal intramolecular electronic couplings for the reaction center should be since it can be argued that both large and small exciton coupling would work equally well. For example, if the interaction between the molecules of the special pair is at least a few times larger than between other pigments, then the special pair transition would occur at the longest wavelength and energy would flow into this state from the antenna and here is where electron transfer would begin. We shall call this the pair coupling case, and it is exemplified by the purple bacterial RC. The opposite situation occurs when all couplings are approximately equal so that exciton states spread over all the RC molecules; this is the multimer case. Possibly PSII is the best example. In this RC there is such a small absorption change from the isolated Chl molecule, 672 to 680 nm, that the interaction between molecules must be small which is consistent with a larger special pair separation than in bacteria. Additionally as the exciton state is initially delocalized the probability of trapping must be enhanced because the state is spatially extended. In either the pair coupling or multimer cases, both static and dynamic disorder in positions and couplings will lead either to partial or complete localization as a result of mixing of the exciton states. The discrete states so produced must then transfer energy by Coulomb and Exchange interaction to the minimum energy state that would be the special pair P1, P2. In other words, fast exciton localization after absorption enables dipole−dipole energy transfer to the lowest state and is the most important effect in enabling trapping by the RC. This should be the case even when the trapping is "trap limited",[20] as the energy must first reach the special pair pigments in order to quench, even if sometimes it revisits the antenna before finally being trapped. In terms of pair coupling or multimer models, PSI appears to be an intermediate case, having a geometry that is not too dissimilar to that of purple bacteria but has electronic interaction similar to PSII.

4. The Effect of Disorder

4.1. Diagonal and Off-Diagonal Disorder and Localization. Structural perturbations cause inhomogeneous broadening in the spectrum via the distribution of static diagonal values, σ_i. The off-diagonal terms, $\delta V_{i,k}$, (eq 4), represent the change in the interaction energy $V_{i,k}$ between molecules i and k compared to the "perfect" structure. This perturbation, which also has a distribution, arises due to irregularity in both positions and orientation of the molecules and contributes to both homogeneous and inhomogeneous line broadening. There are also additional time-dependent fluctuations to the diagonal and off-diagonal terms caused by phonons that describe the effect of protein (lattice) vibrations on the motion of the electron.[37] In the dynamic, off-diagonal case the transfer rate between molecules i and k is modulated by vibrations.

The magnitude of $V_{i,k}$ relative to the dynamic and static disorder energies determine the main characteristics of the exciton motion. If $V_{i,i+1}$ is by far the largest term, the motion is bandlike with the usual extended Bloch states. If static disorder is large then variation in a molecule's position or orientation leads to the range of transition energies ($E_i + \sigma_i$) and exciton transfer energies ($V_{ik} + \delta V_{ik}$) becoming important. If positional fluctuations are so large that they overcome the delocalizing effect of the average exciton coupling, $\langle V_{ik} + \delta V_{ik}\rangle_{av}$, then localization occurs,[37] i.e., when $\langle\sigma\rangle_{av}$ is greater than $\langle V_{ik} + \delta V_{ik}\rangle_{av}$.

Using eq 4 the spectrum of the RC was satisfactorily simulated with a diagonal disorder of 350 cm^{-1} and an off-diagonal disorder of 100 cm^{-1} and compared well to that spectrum simulated from the eigenvalues without disorder as was done to obtain Figure 2. Hole-burning studies on PSI, but at 1.6 K, indicate a inhomogeneous line width of 100 cm^{-1} [38] smaller than our estimate; possibly this result is caused by narrowing due to the exciton coupling. The calculated disorder energies obtained are similar to, but larger than, those calculated for the LHII complex of *Rb. sphaeroides*, 230 and 110 cm^{-1},[39] and PSII, 210 cm^{-1}.[17]

The method of Fidder et al.[29] can also be used to calculate the density of states, excitation energy, oscillator strength, and exciton localization in the RC as a function of both wavelength and magnitude of disorder. For example, the mean oscillator strength f_{av} varies across the absorption band and may be calculated from the single photon transition dipole $f_n = \sum_{i=1}^{N}(a_{i,n}\mu_i)^2$, where μ is the transition moment for the Q_y transition. The inset in Figure 6 shows f_{av} relative to Chl vs wavelength. In the neutral RC it is constant at 0.15 below 660 nm and then increases steadily to 1.5 at 690 nm, the lowest exciton states thus having gained oscillator strength. This increased oscillator strength implies that superradiance may be possible in the PSI RC; however, it will be difficult to observe not only because the value of f is about two times smaller than that observed in the LHII complex at room temperature[40] but also because there are always many, typically more than 40, antenna chlorophylls associated with the RC which will emit at similar wavelengths. In P_{700}^+, f_{av} is ~0.12 below 670 nm, but then it rises to only 1.15 at 680 nm, which reflects the more localized nature of this exciton state compared to that of P_{700}.

The average dipole strengths and energies vs diagonal disorder energy are shown in Figure 6. The off-diagonal coupling was kept constant, and as the frequency of light absorption exceeds the relaxation rates among the exciton states the diagonal disorder was treated as being static. The appearance of these average dipole strengths and energies is similar

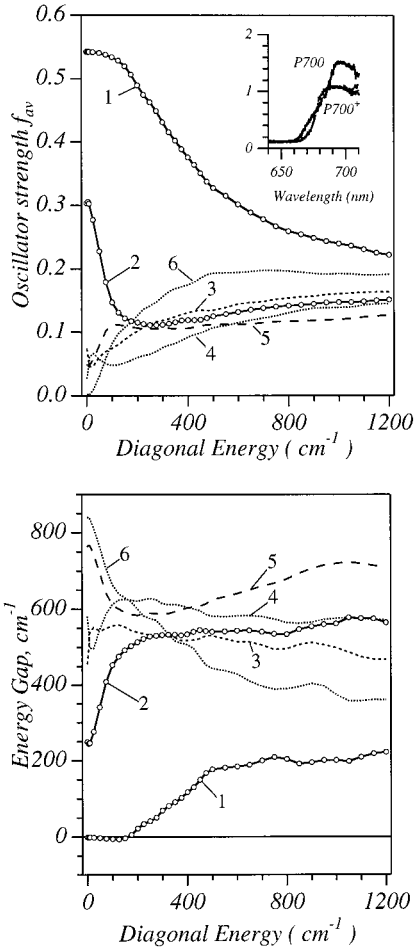

Figure 6. (A) Normalized averaged oscillator strength $f_{av} \equiv \langle f \rangle / \Sigma^6_1 \langle f \rangle$ and (B) energy gap (cm^{-1}) from state 1 vs diagonal disorder, σ (cm^{-1}), sampled from a Gaussian distribution. Data labeled 1 represents the lowest energy exciton state, 6 the highest. (Inset) The oscillator strength for P_{700} and P_{700}^+ transitions vs wavelength at a disorder of 350 cm^{-1} and relative to Chl with $f = 1$.

in general form to, but different in detail from that, calculated for the more ordered LHII antenna of purple bacteria.[41] In that antenna its high symmetry ensures that the eigenstates move apart as diagonal disorder is increased and the oscillator strengths increase for the forbidden lowest state and decrease for the next two states. The lower approximately C_2 symmetry of PSI means that the exciton states are mixed in a more erratic manner than in LHII. The mixing causes the exciton states 1 and 2 (Figure 6), which are lowest in energy, to lose oscillator strength and the higher energy and weaker states to gain in strength. States 2 to 6 tend to group together in energy as disorder is increased, but state 1 remains distinct from the others up to ~500 cm^{-1} of disorder. Inspecting the eigenvectors shows that this state is, however, still mixed with others. The result of these changes in oscillator strength and energy imply that a only small amount of disorder, 200−500 cm^{-1}, will alter the absorption profile of the RC, which then becomes less sensitive to its further increase.

As the disorder σ becomes comparable to the electronic coupling U the eigenstates become localized. One measure of this localization[29] is the "participation number" at energy E and disorder σ and is defined as

$$L(E)_\sigma^{-1} = N\rho(E)\langle \sum_j \delta(E - U_j) \sum_i a_{ij}^4 \rangle^{-1} \qquad (5)$$

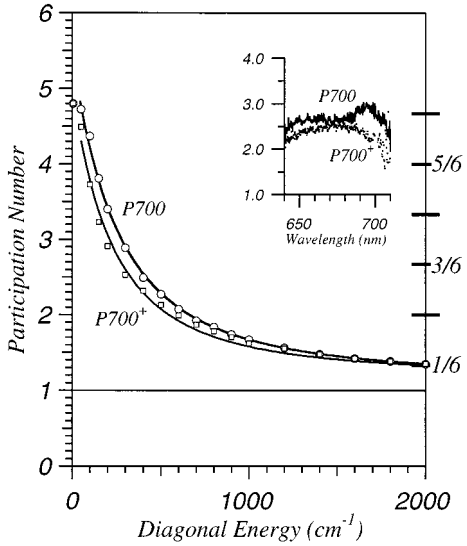

Figure 7. Exciton localization participation number L_σ^{-1} vs diagonal disorder σ (cm^{-1}) for P_{700} and P_{700}^+. The fits to the data points, except the first, are Lorenzians. The ideal and fractional localization is given by $2(N + 1)/3$ and is shown at the right of the graph. (Inset) Localization vs wavelength with $\sigma = 350$ cm^{-1}.

where $\rho(E)$ is the density of states at energy E, U_j is the energy eigenvalue for state j, and $a_{i,j}$ are the eigenvector coefficients for each molecule in that exciton state and the angular brackets indicate Monte Carlo averaging. The value of $L(E)^{-1}$ for the neutral RC is almost constant over the absorption band from ~640 to ~680 nm but peaks slightly at ~690 nm, see inset of Figure 7. For P_{700}^+ the participation number is more symmetrical with wavelength and decreases from 2.4 in the band center to 2.0 at the band edges, a smaller value than P_{700} that presumably reflects the more localized nature of this exciton.

The participation number averaged over the energy is $L_\sigma^{-1} = \langle L(E)_\sigma^{-1} \rangle_E$ and has consequences for the nature of the exciton state in the RC. Electronically isolated molecules would produce a value of 1, and coupled molecules with no disorder have a value of $2(N + 1)/3$ or 4.67 for the $N = 6$ molecules in the RC. We find that as σ increases L_σ^{-1} decreases as the exciton becomes more localized, see Figure 7. At $\sigma = 0$ the participation ratio is 4.8, very close to that predicted theoretically, and falls to 1.2 at $\sigma = 3000$ cm^{-1}, essentially the single molecule limit. At 350 cm^{-1}, the typical P1−P2 coupling energy, the participation number is 2.7 indicating that the exciton has considerable delocalization effectively over three molecules or half the RC. It is, however, not clear how the participation ratio relates to the average number of molecules of a certain excitonic transition except that this ratio seems to give a larger number than inspection of the spread of the wave function.[40]

An alternative measure of localization is the correlation length ξ_σ defined as[42,43]

$$\xi_\sigma^2 = \sum_{ij} \langle \Delta_{ij} \rangle_\sigma r_{ij}^2 / \sum_{ij} \langle \Delta_{ij} \rangle_\sigma \qquad (6)$$

where Δ_{ij} is the quantum connectivity between molecules i and j is given by $\Delta_{ij} = P_{ij}/(P_{ii}P_{jj})^{1/2}$, where $P_{ij} = \sum_k a_{ik}^2 a_{jk}^2$. The separation between any two molecules is r_{ij}, and the angular brackets again indicate averaging. At $\sigma = 350$ cm^{-1} the correlation length ξ is 14.5 Å. To compare this with the structure we note that the special pair are separated center-to-center by 6.5 Å and the equivalent distances to the accessory Chls are 12.8 (P2−C4, Figure 1) and 13.2 Å (P1−C3). Thus

a correlation length of 14.5 Å approximately covers the special pair and one other molecule, which is consistent with the value of L_σ^{-1} of ~3.

4.2. Comparison of Reaction Centers. The RC's for purple bacteria, PSI, and PSII fall into two or possibly three categories as described briefly above. The coupling in purple bacteria is so large that the special pair is the source of the electron transfer even though in modified RC's this can be altered if the redox potential is changed.[44] As the special pair coupling is large compared to *kT* at room temperature, the lowest exciton state should be mainly localized on the special pair and be less sensitive to disorder than is PSII or PSI. In PSII the separation between the special pair is thought to be not that much less than that between pairs of other pigments and is possibly in the region of 8−12 Å so that the pairwise couplings are all similar, and it is not clear where disorder will localize the exciton state. Small couplings, estimated[17] as ~100 cm^{-1}, are expected in PSII as the P_{680} absorption is not much shifted from that of isolated Chl molecules. In PSI the couplings are also similar between near neighbors so that disorder will localize the exciton state onto P1 and P2 as the lowest state contains this special pair of molecules.

4.3. Time Dependence. A natural question to ask is how will the exciton coupling influence the subsequent electron-transfer processes. The effects of static disorder as described above leads to a mixing and hence localization of the exciton states, but the disorder must also have a time-dependent contribution. This itself can have three parts, first a rapid dephasing, secondly equilibration among the exciton states and then intramolecular energy redistribution (IVR), which can compete with equilibration. The initially prepared pure state is a coherent superposition of the stationary exciton states only if the exciting laser pulse is short enough that it covers the spectral extent of all exciton transitions. A narrow band laser pulse would, perhaps, only excite one stationary state. The dephasing time of the superposition state can be estimated from the time for energy to transfer between two molecules. In a dimer this is $\tau_{el} \sim \hbar/2\delta E$, which for a 300 cm^{-1} coupling is about 9 fs, but as time progresses the back-and-forth energy transfer will become out of phase as a result of intra- and intermolecular vibrational motion or other interactions. If we take the time for these processes to be given by the corresponding experimental bandwidth of the P_{700} transition, ~200 cm^{-1}, this time is similarly short, about 13 fs. Thus the coupling produced by the excitation process would be destroyed by motions of the protein matrix within very few transfer periods.[45] What remains now are the exciton states as shown in Figure 3B and which by energy transfer, for example, must equilibrate with one another. Because of the considerable overlap of the transitions and the proximity of the molecules the energy transfer[39] must be very rapid and in the region of ~100 fs. The final result will be a more localized exciton such as described by the participation number. It seems probable that electronic dephasing and localization of the PSI RC exciton state will occur well before electron transfer, which takes slightly less than 1 ps.[20]

5. Conclusions

The calculated exciton coupling in the PSI reaction center does not vary much between near neighbors in the RC and is 330 cm^{-1}. This result suggests that the state giving rise to the absorption of the special pair is partly extended over the other molecules in the RC but will be localized by disorder. This localization is estimated to occur before primary electron transfer. The experimental $P_{700}^+ - P_{700}$ and $A_0^- - A_0$ spectra are well-described by the exciton coupled model based on the X-ray structure provided that the molecules are rotated in their plane so that the angle between the "special pair" Q_y dipoles is about 40°. Displacing and separating the special pair by more than $\pm^1/_2$ Å away from the X-ray coordinates worsens the fit of the calculated and experimental difference spectra.

Acknowledgment. I am most grateful to Dr. N. Krauss for providing the PSI X-ray coordinate data prior to publication, to Drs. Peter Heathcote and Gavin Reid for many helpful discussions, and also to Dr. Jo. McDouall for the initial Gaussian94 calculations. The support of the BBSRC and EPSRC is acknowledged.

References and Notes

(1) Fromme, P.; Witt, P.; Schubert, W. D.; Klukas, O.; Saenger, W.; Krauss, N. *Biochem. Biophys. Acta* **1996**, *1275*, 76.
(2) Schubert W D.; K. O.; Krauss N.; Saenger W.; Fromme P.; Witt, H. T. *J. Mol. Biol.* **1997**, *272*, 741.
(3) Parson, W. W.; Warshel, A. *J. Am. Chem. Soc.* **1987**, *109*, 6152.
(4) Scherer, P. O.; Fischer, S. F. *J. Phys. Chem.* **1989**, *93*, 1633.
(5) Scherer, P. O. J.; Fischer, S. F. *Chem. Phys. Lett.* **1997**, *268*, 133.
(6) Warshel, A.; Chu, Z. T.; Parson, W. W. *J. Photochem. Photobiol. A* **1994**, *82*, 123.
(7) Alden, R. G.; Parson, W. W.; Chu, Z. T.; Warshel, A. *J. Am. Chem. Soc.* **1995**, *117*, 12284.
(8) Alden, R. G.; Parson, W. W.; Chu, Z. T.; Warshel, A. *J. Phys. Chem.* **1996**, *100*, 16761.
(9) Thompson, M.; Zerner, M. *J. Am. Chem. Soc.* **1991**, *113*, 8210.
(10) Thompson, M. A.; Zerner, M. C.; Fajer, J. *J. Phys. Chem.* **1991**, *95*, 5693.
(11) Thompson, M. A.; Schenter, G. K. *J. Phys. Chem.* **1995**, *99*, 6374.
(12) Haran, G.; Wynne, K.; Moser, C. C.; Dutton, P. L.; Hochstrasser, R. M. *J. Phys. Chem.* **1996**, *100*, 5562.
(13) Wynne, K.; Haran, G.; Reid, G. D.; Moser, C. C.; Dutton, P. L.; Hochstrasser, R. M. *J. Phys. Chem.* **1996**, *100*, 5140.
(14) Diesenhofer, J.; Epp, O.; Kiki, K.; Huber, R.; Michel, H. *J. Mol. Biol.* **1984**, *180*, 385.
(15) Huber, R. *Angew. Chem., Int. Ed. Engl.* **1989**, *28*, 848.
(16) Beddard, G. S. *Philos. Trans. R. Soc. London A* **1998**, *356*, 421.
(17) Durrant, J. R.; Klug, D. R.; Kwo, S. L.; Grondelle, R. v.; Porter, G.; Dekker: J. P. *Proc. Natl. Acad. Sci. U.S.A.* **1995**, *92*, 4798.
(18) Gouterman, M. *Optical spectra and electronic structure of Porphyrins and related rings*; Academic Press: New York, 1978; Vol. IIIA.
(19) Warshel, A.; Parson, W. W. *J. Am. Chem. Soc.* **1987**, *109*, 6143.
(20) White, N.; Beddard, G. S.; Thorne, J. R. G.; Feehan, T.; Keyes, T.; Heathcote, P. *J. Phys. Chem.* **1996**, *100*, 12086.
(21) Falk, J. E. *Porphyrins and Metalloporphyrins*; Elsevier: Amsterdam, 1964.
(22) Chow, H.; Serlin, R.; Strouse, C. E. *J. Am. Chem. Soc.* **1974**, *97*, 7230.
(23) Frisch, M. J.; Trucks, G. W.; Schlegel, H. B.; Gill, P. M. W.; Johnson, B. G.; Robb, M. A.; Cheesman, J. R.; Keith, T.; Petersson, G. A.; Montgomery, J. A.; Raghavachari, K.; Al-Laham, M. A.; Zakrewski, V. G.; Ortiz, J. V.; Foresman, J. B.; Cioslowski, J.; Stefanov, B. B.; Nanayakkara, A.; Challacombe, M.; Peng, C. Y.; Ayala, P. Y.; Chen, W.; Wong, M. W.; Andres, J. L.; Replogle, E. S.; Defrees, D. J.; Baker, J.; Stewart, J. P.; Head-Gordon, M.; Gonzalez, C.; Pople, J. A. *Gaussian 94*; Gaussian Inc.: Pittsburgh, PA, 1995.
(24) Petke, J. D.; Maggiora, G. M.; Shipman, L. L.; Christoffersen, R. E. *J. Mol. Spectrosc.* **1978**, *73*, 311.
(25) Renge, I. *J. Phys. Chem.* **1993**, *97*, 6582.
(26) Sauer, K.; Lindsay-Smith, J. R.; Schultz, A. J. *J. Am. Chem. Soc.* **1966**, *88*, 2681.
(27) Zandvoort, M. A. M. v.; Wrobel, D.; Lettinga, P.; Ginkel, G. v.; Levine, Y. K. *Photochem. Photobiol.* **1995**, *62*, 299.
(28) Shipman, L.; Housman, D. *Photochem. Photobiol.* **1979**, *29*, 1163.
(29) Fidder, H.; Knoester, J.; Wiersma, D. A. *J. Chem. Phys.* **1991**, *95*, 7880.
(30) Deisenhofer, J.; Michel, H. *Angew. Chem., Int. Ed. Engl.* **1989**, *28*, 829.
(31) Webber, A.; Su, H.; Bingham, S. E.; Kass, H.; Krabben, L.; Kuhn, M.; Jordan, R.; Schlodder, E.; Lubitz, W. *Biochemistry* **1996**, *35*, 12857.
(32) Mathis, P.; Ikegami, I.; Setif, P. *Photosynth. Res.* **1988**, *16*, 203.
(33) Hastings, G.; Hoshina, S.; Webber, A. N.; Blankenship, R. E. *Biochemistry* **1995**, *34*, 15512.
(34) Small, G. J. *Chem. Phys.* **1995**, 239.

(35) Kwa, S. L. S.; Eijckelhoff, C.; Grondelle, R. v.; Dekker, J. P. *J. Phys. Chem.* **1994**, *98*, 7702.

(36) Fujita, I.; Davis, M. S.; Fajer, J. D. *J. Am. Chem. Soc.* **1978**, *100*, 6280.

(37) Pope, M.; Swenberg, C. E. *Electronic Processes in Organic Crystals*; OUP: Oxford, 1982.

(38) Gillie, J. K.; Lyle, P. A.; Small, G. J.; Goldbeck, J. H. *Photosynth. Res.* **1989**, *22*, 233.

(39) Jiminez, R.; Dikshit, S. N.; Bradforth, S. E.; Fleming, G. R. *J. Phys. Chem.* **1996**, *100*, 6825.

(40) Monshouwer R., A. M., van Mourik F., van Grondelle R. *J. Phys. Chem. B* **1997**, *101*, 7241.

(41) Hu, X.; Ritz, T.; Damjanovic, A.; Shulten, K. *J. Phys. Chem. B.* **1997**, *101*, 3854.

(42) Cheng, T. M.; Bauer, J. D.; Skinner, J. L. *J. Chem. Phys.* **1990**, 8973.

(43) Skinner, J. L. *J. Phys. Chem.* **1994**, *98*, 3.

(44) Brederode M., J. M. R., Van-Mourik F. Van-Stokkum I., Van-Grondelle R. *Biochemistry* **1977**, *36*, 6855.

(45) Forster, T. Delocalised excitations. In *Modern Quantum Chemistry*; Sinanoglu, O., Ed.; Academic: New York, 1965; Vol. III, pp 93−137.

(46) Krauss, N.; Schubert, W. D.; Klukas, O.; Fromme, P.; Witt, H. T.; Saenger, W. *Nat. Struct. Biol.* **1996**, *3*, 965.